

Calibration of the Relationship between Precipitable Water Vapor and 225 GHz Atmospheric Opacity via Optical Echelle Spectroscopy at Las Campanas Observatory

Joanna Thomas-Osip,¹ Andrew McWilliam, M. M. Phillips¹, N. Morrell¹ and I. Thompson

*The Observatories of the Carnegie Institute of Washington
813 Santa Barbara St, Pasadena, CA 91101*

jet@lco.cl, andy@ociw.edu, mmp@lco.cl, nmorrell@lco.cl, ian@ociw.edu

T. Folkers

Arizona Radio Observatory, University of Arizona, Tucson AZ 85721, USA

tfolkers@hamms.as.arizona.edu

T. Folkers

*Physics Department and Astronomy Department
University of Michigan, Ann Arbor, MI 48109*

fca@umich.edu

and

M. Lopez-Morales

*Carnegie Institution of Washington, Department of Terrestrial Magnetism
5241 Broad Branch Road, NW, Washington, DC 20015*

mercedes@dtm.ciw.edu

ABSTRACT

We report precipitable water vapor (PWV) measurements made at Las Campanas Observatory using optical spectra of H₂O lines obtained with the Magellan echelle spectrograph, and calculated using a robust technique that is accurate to 5-10%. Calibration of the relationship between our PWV measurements and opacity values at 225 GHz was

¹Las Campanas Observatory, Colina El Pino, Casilla 601, La Serena, Chile

made possible by simultaneous tipping radiometer observations. Based on this calibration, we present Las Campanas Observatory winter-time precipitable water vapor statistics, measured using the tipping radiometer, during a two month campaign. The median value of 2.8 ± 0.3 mm is consistent with that measured at the nearby La Silla Observatory during the VLT site survey. We conclude that, in the Southern hemisphere winter months, we can expect good conditions for infrared observing ($\lesssim 1.5$ mm) approximately 10% of the time at Las Campanas Observatory.

Subject headings: radio lines: general — site testing — techniques: spectroscopic

1. Introduction

As part of the Giant Magellan Telescope site testing program at Las Campanas Observatory, we are interested in characterizing precipitable water vapor due to its impact on mid-IR observations through decreased transparency, increased thermal-IR background, and the introduction of extraneous spectral features. In this study, we report on our efforts to absolutely calibrate the relationship between 225 GHz opacity and precipitable water vapor (PWV).

The opacity at 225 GHz has been shown to be directly related to the column of precipitable water vapor in the atmosphere (c.f. Plambeck 1978; Chamberlin & Bally 1995; Davis et al. 1997). The relationship, however, is also a function of pressure (and therefore altitude) and temperature due to the fact that the 225 GHz opacity derives from the wing of a strong water vapor absorption line at 183 GHz arising from the 3-2 rotational transition (Waters 1976) where the wings are mostly due to pressure broadening. Efforts to calibrate this relationship have taken several different forms including deducing the column of PWV from a model of the atmospheric transmission at mm wavelengths and measuring the PWV using radiosonde type devices. Comparison between methods can be complicated by the effects of other atmospheric constituents (e.g. O_3 , O_2 , and N_2) on the dry air opacity.

Swings et al. (1990) combined high resolution echelle spectroscopy of a water vapor line at 6943.79 \AA with a technique devised by Brault, Hall, & Fender (1975) (henceforth B75) to calibrate mid-infrared sky radiance measurements obtained at the La Silla Observatory during the VLT site survey. Through the use of modern partition functions and the addition of 13 new optical lines for PWV measurement, we have improved substantially on the B75 method when used in conjunction with high resolution echelle spectroscopy. Section 2 describes the method in detail and our results using it. Our campaign to measure the 225 GHz opacity using a tipping radiometer, the resulting calibration and PWV statistics for Las Campanas Observatory are presented in § 3.

2. Optical Echelle Spectroscopy

The Magellan echelle spectrograph (MIKE) was used to acquire spectra of rapidly rotating A and B stars in the visual magnitude range 4.0 to 6.0. Due to the high continuous opacity these hot stars show very few absorption lines, particularly in the red optical region. Furthermore, their high rotational velocities ensure that any extant stellar lines are rotationally broadened, to widths much larger than lines arising from absorption through the earth’s atmosphere.

The Las Campanas Observatory site monitoring program includes a list of 16 telluric standard stars¹ that pass close to the zenith, such that at any time one, or more, stars are within 2 hours of the meridian. Observers were instructed not to submit echelle spectra taken through cirrus clouds as a precaution against spurious PWV measurements arising from clumpy clouds.

Typically, spectra were acquired when the hot stars were close to the zenith. The spectral resolving power was normally $\sim 40,000$ with S/N in excess of 100:1. The echelle spectral format offers the advantage that light of a given wavelength occurs in two consecutive orders. This permits independent measurement of each line in two orders, providing that the lines fall on the echelle CCD array and there is sufficient signal.

Reductions of the raw spectra were performed using the MIKE Pipeline reduction software, written by Dan Kelson, using algorithms outlined in Kelson et al. (2000), Kelson (2003) and Kelson (2006).

While the site survey program, including the measurement of PWV, is on-going, this paper is based on measurements of 15 spectra, taken on 15 nights from 21 July to 21 November 2005. The Tipper was not operational on every night that echelle spectra were taken; thus, our Tipper calibration is based on 11 of the 15 spectra.

Figures 1 and 2 show the spectrum near the H₂O line used by B75 at 6943.79 Å, in consecutive orders on our driest and wettest nights. The equivalent widths of the line in these spectra ranges from 5 to 52 mÅ.

2.1. Analysis of the Spectra

Following B75, we analyze our spectra using a robust and computationally simple method, but we employ improved partition functions that result in a slightly different choice of line excitation potentials than B75. We have also added five new weak optical lines that may be used for reliable PWV estimates.

B75 pointed out that for a given temperature there is a certain, unique, energy level which

¹<http://www.lco.cl/lco/operations-inf/gmt-site-testing-1/stars-for-measuring-pwv-with-mike/stars-for-measuring-pwv>

corresponds to a temperature-insensitive absorption coefficient. This follows from the Boltzmann equation (Equation 1) describing the population of the energy levels of atoms and molecules: at any given temperature, T , the population of levels with a unique excitation potential matches the sensitivity of the partition function to temperature; in this case the fractional population of the level (n_i/N_{tot}) is approximately constant with T ,

$$\frac{n_i}{N_{\text{Tot}}} = \frac{g_i e^{-EP_i/kT}}{Q(T)} \quad (1)$$

where the partition function, $Q(T)$, is given by

$$Q(T) = \sum g_j e^{-EP_j/kT}$$

In Figure 3 we show a plot of (n_i/N_{tot}) versus temperature for three different energy levels, over a range of temperatures expected in the earth’s atmosphere; the plots were calculated using Equation 1, and are normalized to a temperature of $T=270$ K. Figure 3 is similar to Figure 1 in B75, but here we have used the partition function taken from the Kurucz² website that we believe is more appropriate than the simple approximation for the H₂O partition function employed by B75. Figure 3 indicates that for levels with excitation energy in the range 225–300 cm⁻¹ the ratio (n_i/N_{tot}) varies by less than $\sim 5\%$ over the temperature range from 220 to 300 K. The excitation energy range least sensitive to atmospheric temperature, around 270–280 cm⁻¹, is slightly higher than the value of 225 cm⁻¹ indicated by B75, and probably results from our use of modern partition functions. We note that even the $\sim 5\%$ uncertainty could be reduced by use of a weighted average of the results from lines spanning the critical range of excitation energies.

Figure 4 shows a MSIS-E-90³ model atmosphere for Las Campanas Observatory on one of the nights for which we have a PWV spectrum; it can be seen that the temperature range of the model is covered by the range in Figure 3. The largest temperature deviation from 270 K, in the model, is 210 K and occurs at the tropopause between 10 and 20 km height; it encompasses approximately 20% of the mass of the atmosphere. We note that the water vapor pressure above ice, or water, at 220 K is approximately 0.6% of the vapor pressure at 270 K (e.g. Mason 1971). Thus, if the H₂O is uniformly distributed through the atmosphere we estimate that approximately 0.1% of the mass of the atmospheric water vapor lies in the 10–20 km region, where the temperature differs most from 270 K. In other words the coolest region of the atmosphere contains a negligible fraction of the total water vapor, and thus even the small systematic deviation of n_i/N_{tot} from this region will be reduced to insignificance compared to the whole atmosphere. We conclude that lines with excitation levels near 270–280 cm⁻¹ can provide very robust estimates of the atmospheric PWV.

²<http://kurucz.harvard.edu/>

³<http://modelweb.gsfc.nasa.gov/models/msis.html>

Under the assumption of pure absorption radiative transfer, and a constant line profile function through the earth’s atmosphere, B75 pointed out that the PWV, in cm, is given by:

$$PWV = L/SX \quad (2)$$

where L is the log flux, S is the line strength parameter, and X is the airmass. B75 referred to L as the “log equivalent width”, and defined it as the the integral of the natural log of the flux removed from the continuum by the line:

$$L = \int_{-\infty}^{\infty} -\log_e \left(\frac{I(\nu)}{I_c} \right) d\nu$$

The line strength parameter S depends on atomic parameters as follows:

$$S = gf \left(\frac{\pi e^2}{mc} \right) \frac{e^{-EP/kT}}{Q(T)} \left(\frac{N_A}{A_{H_2O}} \right) \quad (3)$$

Note that the gf value can be calculated from the Einstein spontaneous emission coefficient, A_{ul} , by the following relation:

$$gf = 1.4992\lambda^2 g_{up} A_{ul}$$

where λ is in cm and A_{ul} is in Hertz.

In Equation 3 N_A is Avogadro’s number, 6.022×10^{23} , and A_{H_2O} is the atomic mass of H_2O , at 18.0. Note that use of Equation 3 will give PWV, in cm, if the log flux integration, L, is performed over the frequency spectrum of the line in Hertz units. For an assumed temperature of 270 K, which is our single model atmosphere parameter, Equation 3 reduces to:

$$S_{270} = \frac{2.917335 \times 10^8}{\sigma_{vac}^2} A_{ul} g_{up} e^{-EP/187.6524} \quad (4)$$

In Equation 4 we have applied the additional factor $-c\sigma_{vac}^2$ (where σ_{vac} is the vacuum wavenumber) in the calculation of the strength factor, S, to account for the line flux measured in Kaysers (cm^{-1}), consistent with the S factors given in B75.

In practice the line profile depends most strongly on the atmospheric pressure, which is a function of height, so a constant line profile condition, mentioned by B75, does not apply. However, in the case of unsaturated lines, the line profile does not affect the total absorbed flux, and Equation 2 becomes valid, even with large variations in the line profile through the atmosphere. In this study we computed PWV values from our measured H_2O line log fluxes, with wavelengths in cm^{-1} units,

using Equations 2 and 4; this is correct for unsaturated lines. For saturated lines the variability of the line profile with height signals the break-down of Equation 2. In this case, to properly measure PWV would require a model atmosphere that accounts for the relation between line profile and column mass of H₂O.

B75 measured the line strength parameter, S , using the McMath Solar Telescope for numerous lines with excitation near 225 cm^{-1} , mostly for lines in the near-infrared region of the spectrum. However, B75’s list did include one line in the optical, at 6943.79 \AA . As a check of the B75 value of S for this line, we computed S from the Kurucz⁴ gf value using Equation 4. The Kurucz gf value, which was taken from theoretical predictions of Partridge & Schwenke (1997), leads to a value of S which is $\sim 60\%$ higher than the B75 measurement, although there is reason to suspect the veracity of this result since the relative Kurucz gf values appear to be inconsistent with the appearance of lines in our telluric spectra.

Given this disagreement, we decided to check the result from the 6943.79 \AA line by identifying additional optical H₂O lines with excitation energies near $270\text{--}280\text{ cm}^{-1}$ and reliable, measured, gf values. Our criteria for selecting the additional lines also included the requirement that they have a strength that could be measured in our spectra, but not so strong that they might be saturated, and that the lines be clear from blends, including H₂O lines and other lines present in our telluric spectra (e.g. from the O₂ molecule). We searched the HITRAN⁵ database of H₂O line parameters for suitable lines and visually inspected our telluric spectra to check for non H₂O blends.

In Table 2 we show line parameters for the 6943.79 \AA line of B75 and 5 new weak lines identified in this work. The HITRAN database included optical H₂O line gf values from a variety of sources. The gf values for our lines in Table 2 came from Coheur et al. (2002), measured using a high resolution spectrograph and a controlled, fixed, water vapor path. For the 8 strong H₂O lines listed in Table 4 that were used for the saturation investigation (see § 2.3), the gf values were taken from Coheur et al. (2002) and similar laboratory measurements of Brown, Toth, & Dulick (2002). For the 6943.79 \AA line the empirical Coheur et al. (2002) gf value indicated a line strength parameter, S , that agreed with the B75 value to within 1%. Given the good agreement between the experimentally determined S factors, and the difficulty in making theoretical gf predictions for weak lines (due to small overlap of the level wavefunctions), we chose not to use the Kurucz H₂O gf values.

2.2. Results of Optical PWV Measurements

The range of line equivalent widths, in m\AA , for our list of temperature insensitive H₂O lines is indicated in Table 2. Table 3 shows the log line fluxes and the resultant PWV values computed

⁴<http://kurucz.harvard.edu/>

⁵<http://cfa-www.harvard.edu/HITRAN/>

using Equations 2 and 4 (multiplied by 10 to get PWV in mm). The PWV values range from 1 to 7mm for the 15 nights, and there is good agreement, typically $\sim 10\%$, between the results for each line. This dispersion is consistent with the accuracy of the measured line gf values: good gf values are usually accurate to 5 to 10%. The weakest line in Table 2 is at 5954.9 Å, and is most reliable on nights with more than ~ 5 mm PWV. The strongest line in Table 2, at 7287.4 Å, is useful for measuring PWV on very dry nights; on wet nights it will be the first line to become saturated.

In Figure 5 we compare the individual PWV results for each line with the average for each spectrum. The figure shows no clear systematic differences between the PWV values for the individual lines. The rms scatter of the individual line PWV measurements about the mean for each spectrum is 0.3mm H₂O on average, corresponding to $\sim 10\%$.

In Figure 5 the 7287.4 Å point for the wettest night appears below the main correlation, slightly more than might be expected from the general scatter of the points. In addition to this for the next two most wettest nights the 7287.4 Å PWV points are also the lowest of the 6 lines used. Although these differences are extremely subtle, and could easily be random, they may indicate the beginning of saturation in the 7287.4 Å line; indeed, the expected effect of saturation is to reduce the computed PWV from Equations 2 and 4. If that is the case then the strength of our 7287.4 Å line on the wettest night, at 134 mÅ, represents the useful upper limit for PWV measured using unsaturated H₂O lines under the assumption of no saturation.

The method used to measure PWV here could be applied to sites at higher altitude, e.g. Mauna Kea. The lines will be narrower at higher altitude, due to the lower pressure broadening, and thus, saturation will occur at smaller equivalent widths.

2.3. Saturation Investigation

As mentioned earlier, the Brault method used to compute PWV in this paper is quite robust, providing that the lines are not saturated. To use saturated lines for reliable PWV measurement would require a detailed model atmosphere treatment where the run of temperature with PWV, or fractional PWV, is specified through the atmosphere. Given the small scatter in our results it seems likely that all of the lines measured in Table 2 are unsaturated, although the line at 7287.36 Å may be low on our wettest night, indicating the onset of saturation. The use of saturated lines will result in lower computed PWV values, with the error becoming more pronounced with increasing line strength.

It would be useful to know the approximate saturation limit in terms of line strength, so that we do not use overly strong lines in the PWV calculations; this is particularly important for the wettest nights. In order to do this we have made a search for strong H₂O lines in the HITRAN database, with lower level excitation energies in the range 225–300 cm⁻¹ (the range that gives PWV results insensitive to atmosphere temperature). We have calculated the parameters for this list of 8 strong H₂O lines, as shown in Table 4, along with the equivalent widths of each line on our

wettest night (2 August 2005). It is interesting that the stronger H₂O lines tend to lie at redder wavelengths than those in Table 2.

In Figure 6 we show a plot of reduced equivalent width ($REW = \log_{10} EW/\lambda$) for all 14 H₂O lines (from Tables 2 and 4) versus PWV, for the nights of 2 and 20 August 2005, calculated using Equation 2. It is clear that the stronger lines on 2 August give systematically lower PWV values, decreasing roughly linearly with increasing strength; for lines weaker than $REW \sim -4.6$ to -4.7 the PWV values are approximately constant. This saturation limit corresponds to ~ 160 mÅ at 7300 Å; this is larger than the 134 mÅ for the line at 7287.36 Å on the wettest night, which we had previously suspected could be affected by saturation. Therefore, future PWV measurements that use the Brault method should disregard lines above $REW \sim -4.65$. The 20 August points in Figure 6 show that when the lines are below the saturation limit they give results in good agreement; this eliminates the possibility that the decreasing PWV values for strongest lines on the wettest night are due to a systematic error in the line gf values. The unsaturated 20 August points have a standard deviation of 11% in PWV, giving an error on the mean PWV of only 3.3%.

Because line saturation in red giant stars begins around $REW \sim -5.1$ it is clear that the telluric H₂O lines must be more strongly broadened than lines in red giants. Atmospheres of red giant stars are much hotter and have much larger turbulent velocities than the earth’s atmosphere; therefore, the main source of broadening for the telluric H₂O lines cannot be due to temperature or turbulence. The only possibility is that the larger broadening of the telluric lines is due to the much denser earth’s atmosphere (i.e. pressure broadening), for which one would expect the collision frequency and Van der Waals forces to be greater than for lines formed in the low density atmospheres of stars.

Given the larger saturation point for telluric lines, than for stellar lines, the pressure broadening must be overwhelmingly dominant. Thus, it may be that the saturation point changes with atmospheric pressure, for example due to the change in the collision frequency experienced by the H₂O molecules. It is also possible that the saturation point is affected by humidity, both because of the presumably larger H₂O collision cross-section, σv , and also resulting from different Van der Waals forces for H₂O compared to other atmospheric gases.

Future PWV measurements can utilize the stronger H₂O lines listed in Table 4, provided that the saturation limit is not exceeded.

2.4. Temperature Diagnostic

We have attempted to estimate the mean temperature for the wettest night, 2 August 2005, using H₂O lines covering a range of excitation energies. Iterative calculations were performed to find the temperature where the line PWVs matched the temperature-independent PWV value. This mean temperature is actually weighted by the water vapor mass, so it should reflect the temperature closer to the ground, where most of the water vapor lies.

We identified and measured nine lines from the HIRTRAN database with energies ranging from 0 to 756 cm^{-1} . The derived temperatures ranged from 268 K to 290 K, with a mean of 279 K and an rms scatter of 9.5 K. Some of the scatter may have resulted from blending of weak high excitation lines. We note that the mean temperature verifies our use of a temperature of 270 K for the PWV calculations.

Apart from verifying our initial assumption it is not clear how useful the mean temperature diagnostic would be; perhaps it may be used to compare with mass-weighted temperatures calculated from tailored atmosphere models. A better way to compare with theoretical models would be to use profiles of strongly saturated lines to derive the run of temperature with H_2O opacity; but this would require accurate estimates of the line broadening in the theoretical models.

3. 225 GHz Tipping Radiometer Opacity

Opacity at 225 GHz was studied through the use of the University of Arizona Radio Observatory (ARO) 225 GHz Tipping Radiometer (Tipper) on loan to Las Campanas Observatory for the 2005 Southern hemisphere winter season. This radiometer is one of four originally constructed for Millimeter Array site testing purposes by the NRAO and has been in regular use at ARO for sky quality assesment since 1995. These systems have been used to characterize many other sites including Mauna Kea (one of the units has been in operation since 1989 at the Caltech Submillimeter Observatory), Antarctica, Cerro Chanjnantor in Chile, South Baldy and the VLA site in New Mexico (Owen & Hogg 1989; Schwab et al. 1990; Chamberlin 2004).

The characteristics of this radiometer have been extensively described elsewhere (Liu 1987; McKinnon 1987; Chamberlin & Bally 1994) therefore only a short description is provided here. The radiometer is illuminated via a mirror (with a beamwidth of 3.4 degrees) that rotates through 11 elevation angles between an airmass of one and three thus providing a "tip" (measurement of the sky brightness as a function of zenith angle). The beam enters a temperature controlled box in which a chopper wheel allows the receiver to alternately view in repeatable sequences the sky, a cold (45 C) load, the sky, and finally a hot (65 C) load. Use of two different temperature reference loads allows the gain to be measured. The opacity and an estimate of its uncertainty are then derived according to a slab model of the atmosphere from a linear fit to the natural logarithm of the sky brightness temperature as a function of airmass.

Opacities were obtained approximately every 5 minutes continuously between between July 17, 2005 and August 30, 2005 with some exceptions due to storm activity. Of these data, 2999 measurements were selected from the 29 full and partial nights when the conditions were judged to be photometric. The requirement of photometric conditions was imposed not only because of concerns that non-photometric conditions would lead to incorrect fluxes and opacity measurements from the Tipping Radiometer, but also due to the desire to characterize the PWV on nights suitable for mid-infrared astronomy.

3.1. Relationship of 225 GHz opacity to precipitable water vapor

The relationship between 225 GHz opacity, τ , and the column of precipitable water vapor, PWV in mm, can be represented as follows:

$$\tau = \tau_{dry-air} + B \cdot PWV \quad (5)$$

where the opacities and the coefficient B are reported in nepers/airmass and nepers/airmass/mm H_2O , respectively. As used here, a neper is a measurement of attenuation similar to a decibel but based on the natural logarithm, as opposed to base 10.

Plambeck (1978) reports the first estimate of the relationship between τ and PWV. The opacity measurements made at UC Hat Creek Observatory (with an altitude of 1050-m) were correlated with PWV as measured by a radiosonde in Medford, OR (210 km to the NW). Although no values below 4 mm PWV were measured, the coefficient B was found to be 0.06. In the development of the NRAO tipping radiometers, one of which was used in our study, McKinnon (1987) used a similar relationship but included a constant opacity offset of 0.005 nepers/airmass due to absorption by oxygen. They also mention that the relationship is weakly dependent on elevation.

Chamberlin & Bally (1995) report on their calibration efforts in Antarctica using another NRAO tipping radiometer to measure 225 GHz opacities and Radiosonde upper air soundings to measure PWV. Their coefficients can be found in Table 5. A re-analysis of this data is presented by Chamberlin (2004) but does not change the finding of a significant non-zero dry air opacity. The cause of the dry air opacity is not well understood as many atmospheric transmission models (e.g Pardo, Cernicharo & Serabyn 2001; Grossman 1989; Liebe 1989) have failed to reproduce it. A new model that accounts theoretically for the collision-induced absorption by N_2-N_2 molecular partners may be able to resolve this discrepancy (Paine 2004). Further work in understanding and characterizing this parameter is especially important to characterizing the low-precipitable-water-vapor sites at mm wavelengths.

At Mauna Kea this relationship was established in a different way (Davis et al. 1997) and the coefficients can also be found in Table 5. The 225 GHz opacities were measured with the Caltech Submillimeter Observatory (CSO) tipping radiometer, also one of the original NRAO tipping radiometers. The PWV values were obtained through the use of an atmospheric spectral synthesis model called FASCOD2. As the PWV has not been independently measured, it is unclear whether this model might also underestimate the dry air opacity. Given that this calibration is now canonically used to produce PWV values from 225 GHz opacities for Mauna Kea as well as to draw comparisons to other sites, it is important to measure the dry air opacity there.

At Las Campanas Observatory, the precipitable water vapor values determined with the MIKE echelle spectrograph in Section 2.2 and shown in Table 3 were correlated with the 225 GHz opacity measurements as shown in Figure 7. The opacities at the nearest times to those in Table 3 were selected. There was never more than 5 minutes difference and a total of 11 points with times in common were found. A linear relationship was determined using a linear least squares regression

with errors in both the independent and dependent variables. Our coefficients are also listed in Table 5. More points would be needed to better constrain the dry air opacity.

A meaningful comparison of the available calibration coefficients at different sites is made difficult by the lack of uncertainties reported for the calibrations cited in Table 5. Chamberlin & Bally (1995) reported very small uncertainties for their calibration efforts at the South Pole. Their results, however, were superseded by a re-analysis of the tipping radiometer measurements in which the opacities were adjusted systematically upwards by 15% (Chamberlin 2004). No mention of the relative uncertainties was made in Chamberlin (2004) and since adjustments were systematic in nature we will quote the original uncertainty values from Chamberlin & Bally (1995) in Table 5. Regardless of the lack of uncertainties in the reported calibrations, it appears that the dry air opacity decreases with altitude and as expected due to the pressure broadening seen in the wing of the 183 GHz line, the coefficient B , also decreases with altitude. In other words, at lower altitudes (higher pressure) less PWV is required to produce the same opacity at 225 GHz as seen at higher altitudes.

3.2. Calibrated precipitable water vapor at Las Campanas Observatory

Given the calibration determined in the previous section, millimeters of precipitable water vapor and its uncertainty estimate are calculated from the tipper opacities and errors in the following manner:

$$PWV = \frac{\tau - \tau_{dry-air}}{B} \tag{6}$$

$$\sigma_{pwv} = \sqrt{\sigma_{\tau_{dry-air}}^2 + (\tau \cdot \sigma_B)^2 + B \cdot \sigma_{\tau}^2} \tag{7}$$

Figure 8 shows the resulting precipitable water vapor values at night under photometric conditions as a function of time during our campaign. The fraction of the measurements for which PWV was found to be below a given value is displayed in Figure 9. Uncertainties in our PWV estimates are on the order of 10%.

Over the 1.5 month period covered by our measurements, we find a median PWV of 2.8 ± 0.3 mm. Assuming that this time period is representative of the winter PWV characteristics at Las Campanas Observatory, then we can expect good conditions for mid-infrared observing (< 1.5 mm PWV) 10% of the time in winter (c.f. Giovanelli et al. 2001). These results agree well with measurements made at the nearby La Silla Observatory during the VLT site survey (Swings et al. 1990). La Silla is located 24 km south of Las Campanas, and is nearly exactly the same altitude. The VLT site survey measurements were obtained using a mid-infrared sky radiance monitor (Morse & Gillette 1982). The absolute scale of these data was calibrated using the B75 method on coudé spectra of the 6943.79 Å line obtained simultaneously with mid-infrared sky radiance measurements on

several nights.

4. Conclusions

We report on the calibration of the relationship between the column of precipitable water vapor, PWV, and opacity at 225 GHz at Las Campanas Observatory as measured by an NRAO Tipping Radiometer on loan from the University of Arizona Radio Observatory and the high resolution echelle spectrograph, MIKE, on the Magellan Clay Telescope. We have expanded the absolutely calibrated method for measuring PWV using temperature insensitive lines in high resolutions stellar spectra presented by Brault, Hall, & Fender (1975) with improved partition functions and 13 additional lines. We found that optical H₂O lines with reduced equivalent widths weaker than ~ -4.7 to -4.6 are unsaturated and suitable for measuring PWV using the Brault method. This saturation level indicates that the lines are strongly pressure broadened. A calculation of the mass-weighted mean temperature validates the use of a single slab model atmosphere with $T=270$ K to compute PWV values. The linear relationship we found between the MIKE PWV and the 225 GHz opacities is consistent with opacities formed from a pressure broadened wing of the strong water vapor line at 183 GHz and including a dry-air opacity component. The effect of altitude (due to atmospheric pressure changes) is demonstrated by comparing our calibration at Las Campanas Observatory with those few available in the literature. We note the paucity of such absolute PWV calibration efforts and encourage further work especially at sites like Mauna Kea and Paranal where the capability for high resolution echelle spectra already exists.

Based on the relationship determined between the measured PWV and 225 GHz opacities, we find a median PWV of 2.8 ± 0.3 mm and a range between 0.5 mm and 7.5 mm for our two month Southern hemisphere winter time campaign. This is consistent with that measured at the nearby La Silla Observatory during the VLT site survey Swings et al. (1990). Finally, if our campaign is representative of the Southern hemisphere winter months, we can expect good conditions for infrared observing ($\lesssim 1.5$ mm) at the tenth percentile level.

We are grateful to Lucy Ziurys and the Arizona Radio Observatories for the loan of the Tipping Radiometer. We also appreciate Mike Meyer’s help in arranging for the loan. A.M. gratefully acknowledges support from NSF grants AST-96-18623 and AST-00-98612 and I.T. from NSF grant AST-0507325. J.T.-O. thanks John Bally for a particularly fruitful conversation regarding PWV calibration efforts and John Grula for his superb efforts in tracking down obscure references. Finally, we are indebted to Magellan/MIKE observers, Andrea Dupree, Varsha Kulkarni, James Lauroesch, and George Preston, for obtaining spectra.

Facilities: Magellan (MIKE), ARO (Tipper).

REFERENCES

- Brault, J.W., Fender, J.S., & Hall, D.N.B. 1975, *J. Quant. Spec. Radiat. Transf.*, 15, 549.
- Brown, L.R., Toth, R.A., & Dulick, M. 2002, *J. Mol. Spectrosc.*, 212, 57
- Coheur, P.-F., Fally, S., Carleer, M., Clerbaux, C., Colin, R. et al. 2000, *J. Quant. Spec. Radiat. Transf.*, 74, 493.
- Chamberlin, R.A. 2004, *PASA*, 21, 264.
- Chamberlin, R.A. & Bally J. 1994, *Appl. Opt.*, 33,1095.
- Chamberlin, R.A. & Bally J. 1995, *Int. J. Infrared Millimeter Waves*, 16, 907.
- Davis, G. R., Naylor, D. A., Griffin, M. J., Clark, T. A., & Holland, W. S. 1997, *Icarus*, 130, 387.
- Delgado, G., A. Otarola, V. Belitsky, D. Urbain 1999, *ALMA memo* 271.1.
- Giovanelli, R., J. Darling, C. Henderson, W. Hoffman, D. Barry, J. Cordes, S. Eikenberry, G. Gull, L. Keller, J. D. Smith, & G. Stacey 200a, *PASP*, 113, 803.
- Grossman, E. 1989, *A T Program, Ver 1.5, Air Head Software, Boulder CO.*
- Kelson D.D., Illingworth, G.D., van Dokkum, P.G., & Franx, M. 2000, *ApJ*, 531, 159.
- Kelson D.D. 2003, *PASP*, 115, 688.
- Kelson D.D. 2006, *PASP*, *submitted*.
- Liebe, H.J., 1989, *Int. J. Infrared Millimeter Waves*, 10, 631.
- Liu, Z-Y. 1987, *NRAO Millimeter Array Memo* 41.
- Mason, B.J. 1971, “*The Physics of Clouds*” (Clarendon Press)
- McKinnon, M. 1987, *NRAO Millimeter Array Memo* 40.
- Morse, D. & Gillett, F. 1982, *AURA Eng. Report* 73.
- Owen, F.N., & Hogg, D.E. 1989, *Proc. of URSI/IAU Symposium on Radio Astronomical Seeing*, J.E. Baldwin & W. Shouguan, Oxford: Pergamon Press, 42.
- Partridge, H. & Schwenke, D.W. 1997, *J. Chem. Phys.* 106, 4618.
- Paine, S. 2004, *SMA Tech. Memo* 152.
- Pardo, J. R., Cernicharo, J. & Serabyn, E. 2001, *ITAP*, 49/12, 1683.
- Plambeck, R. L. 1978, *IEEE Trans Antennas Propag*, AP-26, 737.

- Schwab, F.R., Hogg, D.E., & Owen F.N. 1990, Proc. of URSI/IAU Symposium on Radio Astronomical Seeing, J.E. Baldwin & W. Shouguan, Oxford: Pergamon Press, 116.
- Swings, J.-P., Appenzeller, I., Ardeberg, A., Charvin, P., Lelievre, G., Perrier, C., Sarazin, M., Schuster, H.-E. & Shaver, P. 1990, VLT Site Selection Working Group Final Report, European Southern Observatory VLT Report No. 62, ed. M. Sarazin
- Waters, J.W. 1976, "Absorption and Emission by Atmospheric Gases" in Methods of Experimental Physics, 12-B, Meeks, M.L. New York: Academic Press, 142.

Table 1. Log of Observations

Obs. #	HR #	UT Date	UT Start	Airmass	Exp. (sec)	Observer*
1	5987	21/Jul/2005	22:49	1.116	24	ALM
2	5987	22/Jul/2005	22:46	1.115	32	ALM
3	806	24/Jul/2005	11:01	1.292	30	ALM
4	5987	25/Jul/2005	01:37	1.033	5	AD
5	845	30/Jul/2005	10:42	1.002	15	IT
6	5517	30/Jul/2005	22:44	1.002	15	IT
7	5517	1/Aug/2005	22:48	1.001	15	IT
8	5517	2/Aug/2005	23:08	1.005	15	IT
9	6930	20/Aug/2005	01:52	1.043	15	GWP
10	5987	20/Aug/2005	23:10	1.011	32	GWP
11	5987	23/Aug/2005	23:08	1.014	62	GWP
12	5987	24/Aug/2005	22:52	1.011	30	GWP
13	6930	15/Sep/2005	01:00	1.098	10	KL
14	8998	21/Nov/2005	23:45	1.030	49	AMcW
15	3034	22/Nov/2005	08:21	1.002	3	NM

*Observer key: AD (Andrea Dupree), IT (Ian Thompson), GWP (George Preston), KL (Kulkarni & Lauroesch), AMcW (Andrew McWilliam), NM (Nidia Morel), ALM (Adams & Lopez Morales)

Table 2. Parameters of Temperature Insensitive H₂O Lines*

σ_{vac} (cm ⁻¹)	λ_{air} (Å)	EP (cm ⁻¹)	gf	S ₂₇₀ (cm ⁻²)	EW _{dry} (mÅ)	EW _{wet} (mÅ)
13717.1744	7288.10	275.50	5.323×10^{-9}	0.2387	6	88
13718.5755	7287.36	300.36	1.251×10^{-8}	0.4912	21	134
13823.1810	7232.21	300.36	5.602×10^{-9}	0.2200	9	75
13894.6353	7195.02	285.42	6.159×10^{-9}	0.2619	12	84
14397.3641	6943.79	224.84	3.059×10^{-9}	0.1795**	5:	52
16788.1104	5954.94	300.36	8.942×10^{-10}	0.03511	...	6

*S and gf values calculated from Coheur et al. (2002) A values.

**Compares well with Brault et al. (1975) S value of 0.180.

Table 3. Line Fluxes* and PWV Values

Obs.	7288.10Å		7287.36Å		7232.21Å		7195.02Å		6943.78Å		5954.94Å [‡]		$\overline{\text{PWV}}^\dagger$ (mm)	σ
	-ln F	PWV	-ln F	PWV										
1	0.036:	1.47	0.047:	1.61	0.041	2.05	1.71	0.30
2	0.032:	1.31	0.031:	1.06	0.028	1.40	1.26	0.17
3	0.039:	1.15	0.019:	0.82	0.99	0.24
4	0.013:	0.53	0.044	0.87	0.023:	1.01	0.0277	1.00	0.027	1.19	0.97	0.30
5	0.122	5.10	0.216	4.39	0.116	4.92	0.126	4.80	0.095	4.92	0.022:	5.26	4.85	0.36
6	0.110	4.60	0.196	3.98	0.101	4.12	0.127	4.84	0.082	4.42	0.015	3.13	4.36	0.32
7	0.093	3.89	0.184	3.74	0.087	3.79	0.100	3.81	0.079	3.68	0.080	3.70	3.77	0.21
8	0.184	7.67	0.293	5.94	0.082	7.17	0.100	7.22	0.060	6.90	0.072	6.84	7.00	0.57
9	0.064	2.57	0.123	2.40	0.151	2.94	0.063	2.31	0.127	2.30	0.122	2.18	2.54	0.35
10	0.063	2.61	0.121	2.44	0.063	2.94	0.067	2.53	0.048	2.45	0.038	...	2.63	0.27
11	0.101	4.17	0.190	3.81	0.066	4.35	0.101	3.80	0.049	3.87	0.040	...	4.03	0.27
12	0.085	3.52	0.158	3.18	0.095	3.64	0.083	3.14	0.068	3.20	0.061	...	3.36	0.30
13	0.040	1.53	0.076	1.30	0.087	1.49	0.040	1.39	0.055	1.60	0.033	...	1.49	0.12
14	0.122:	2.44	0.036	1.63	0.030	2.40	0.030	...	2.10	0.54
15	0.050	2.03	0.094	1.78	0.038	2.19	0.058	2.15	0.037	2.00	0.052:	...	2.05	0.17
					0.052				0.036		0.036			

* Flux measurements for lines appearing in a second order are indicated below the first entry

† Lines appearing in two orders were counted twice for the calculation of the average PWV

‡ The 5954.94Å line was not used for the average PWV

Table 4. Parameters for Strong H₂O Lines

σ_{vac} (cm ⁻¹)	λ_{air} (Å)	EP (cm ⁻¹)	gf	S ₂₇₀ (cm ⁻²)	EW _{wet} (mÅ)
10704.4205	9339.33	300.36	2.730×10 ⁻⁷	10.7240 ²	1047.
11002.2178	9086.55	285.22	1.245×10 ⁻⁸	0.5303 ²	186.
11124.6353	8986.56	300.36	3.017×10 ⁻⁸	1.1852 ²	343.
12254.5139	8157.99	300.36	1.676×10 ⁻⁸	0.6584 ¹	208.
11096.9124	9009.01	285.22	4.443×10 ⁻⁹	0.1892 ²	111.
12238.3078	8168.79	222.05	7.226×10 ⁻⁹	0.4309 ¹	180.
12062.4127	8287.91	224.84	1.770×10 ⁻⁸	1.0397 ¹	313.
12037.5135	8305.05	325.35	2.243×10 ⁻⁸	0.7714 ¹	241.

¹S and gf values calculated from Coheur et al. (2002) A values.

²S and gf values calculated from Brown et al. (2002) A values.

Table 5. Comparison of calibration at LCO to that at other sites

Site	Altitude (km)	$\tau_{dry-air}$	B	Reference
LCO Alcaïno	2410	0.015 ± 0.013	0.076 ± 0.005	this work
S. Pole	2835	$0.026 \pm 0.001^*$	$0.083 \pm 0.002^*$	Chamberlin (2004)
Mauna Kea	4100	0.016	0.05	Davis et al. (1997)
Llanno de Chanjantor	5104	0.0068	0.0407	Delgado et al. (1999)

*uncertainties from Chamberlin & Bally (1995)

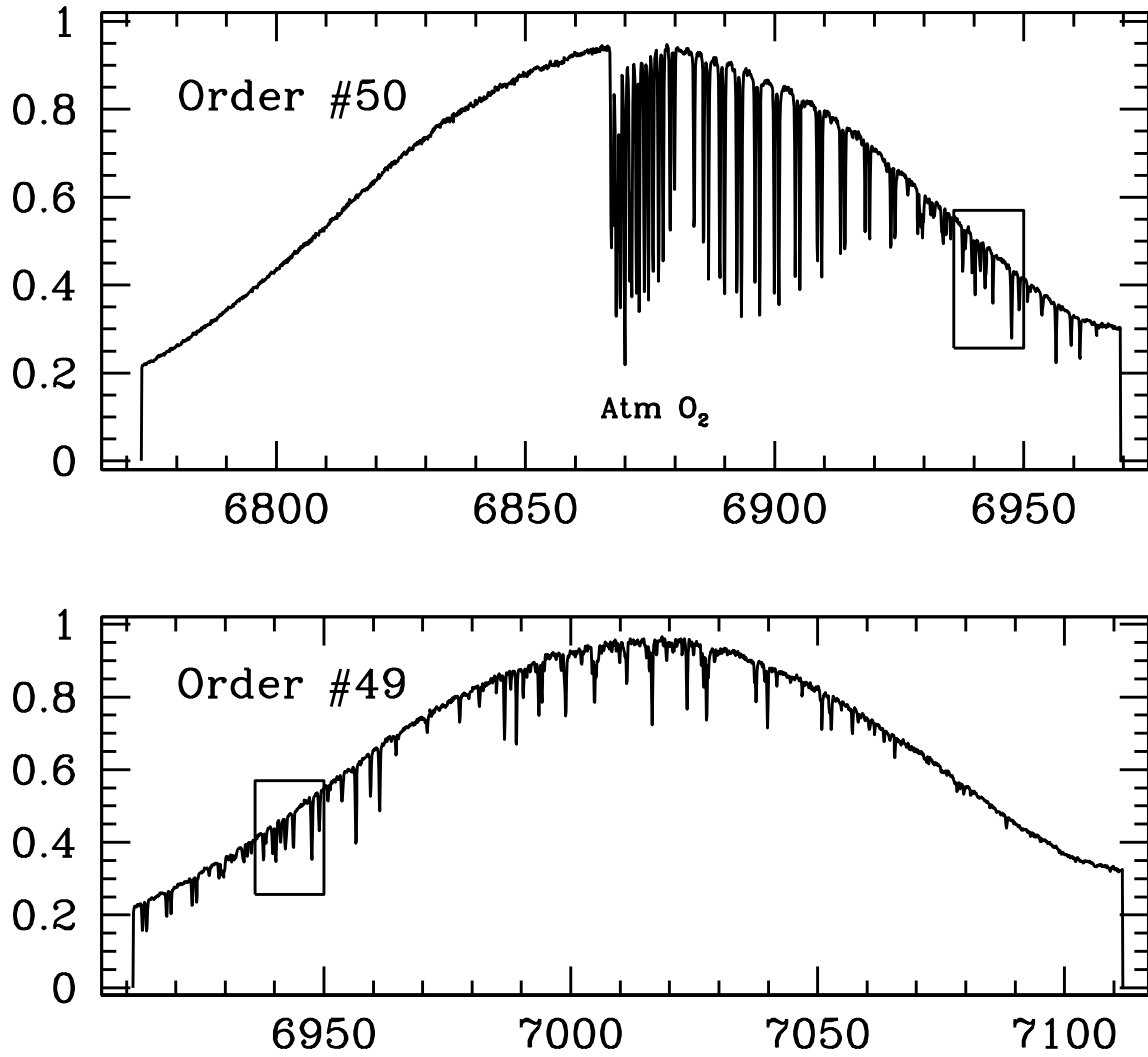


Fig. 1.— Two consecutive orders containing the H₂O line at 6943.78 Å, for a night with 7mm PWV. Boxes indicate the regions shown in detail in the next figure.

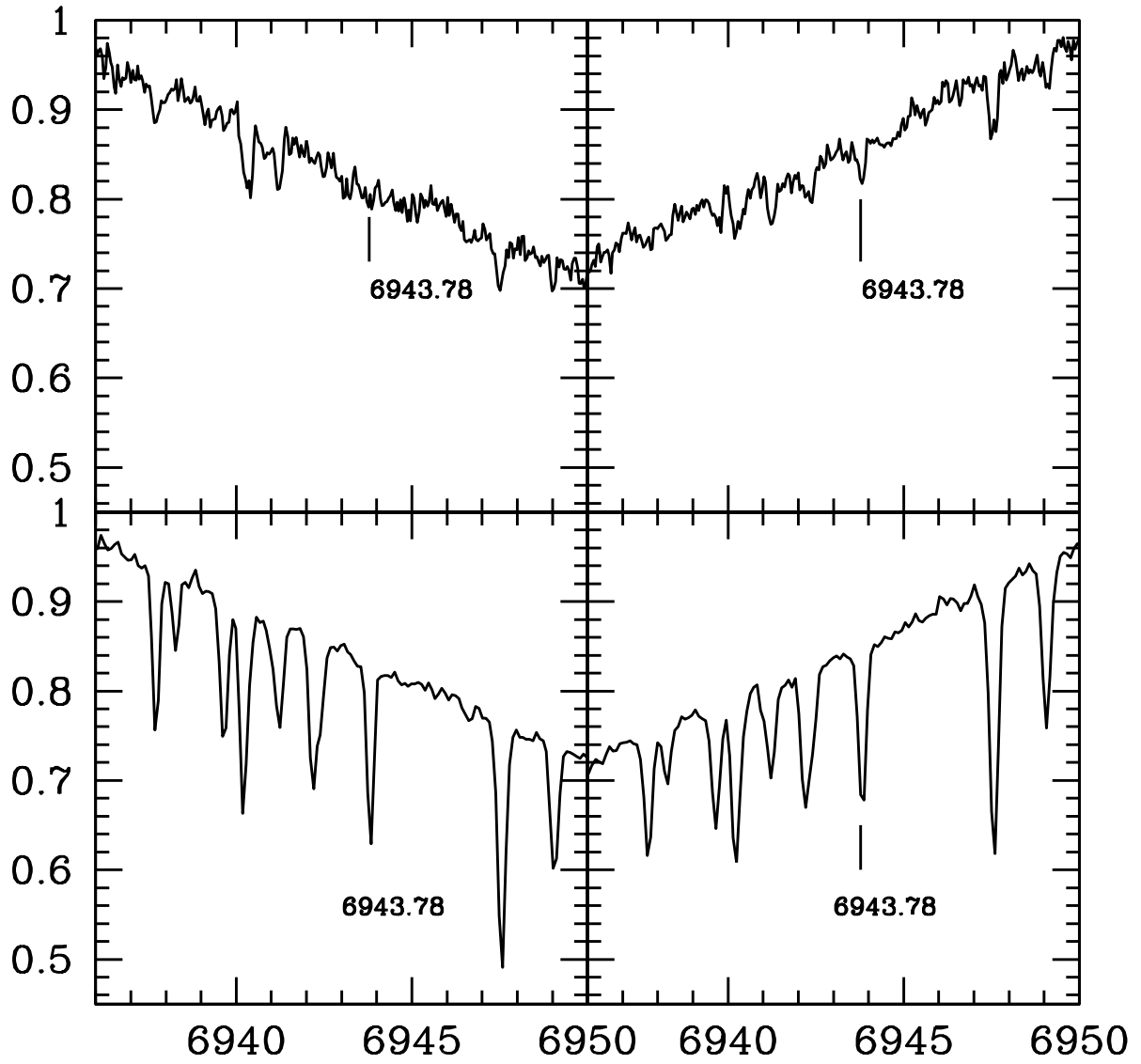


Fig. 2.— A comparison of the 6943.78 Å H₂O line in the two consecutive orders for a dry night, with PWV \sim 1.0mm, and a wet night with PWV \sim 7.0mm.

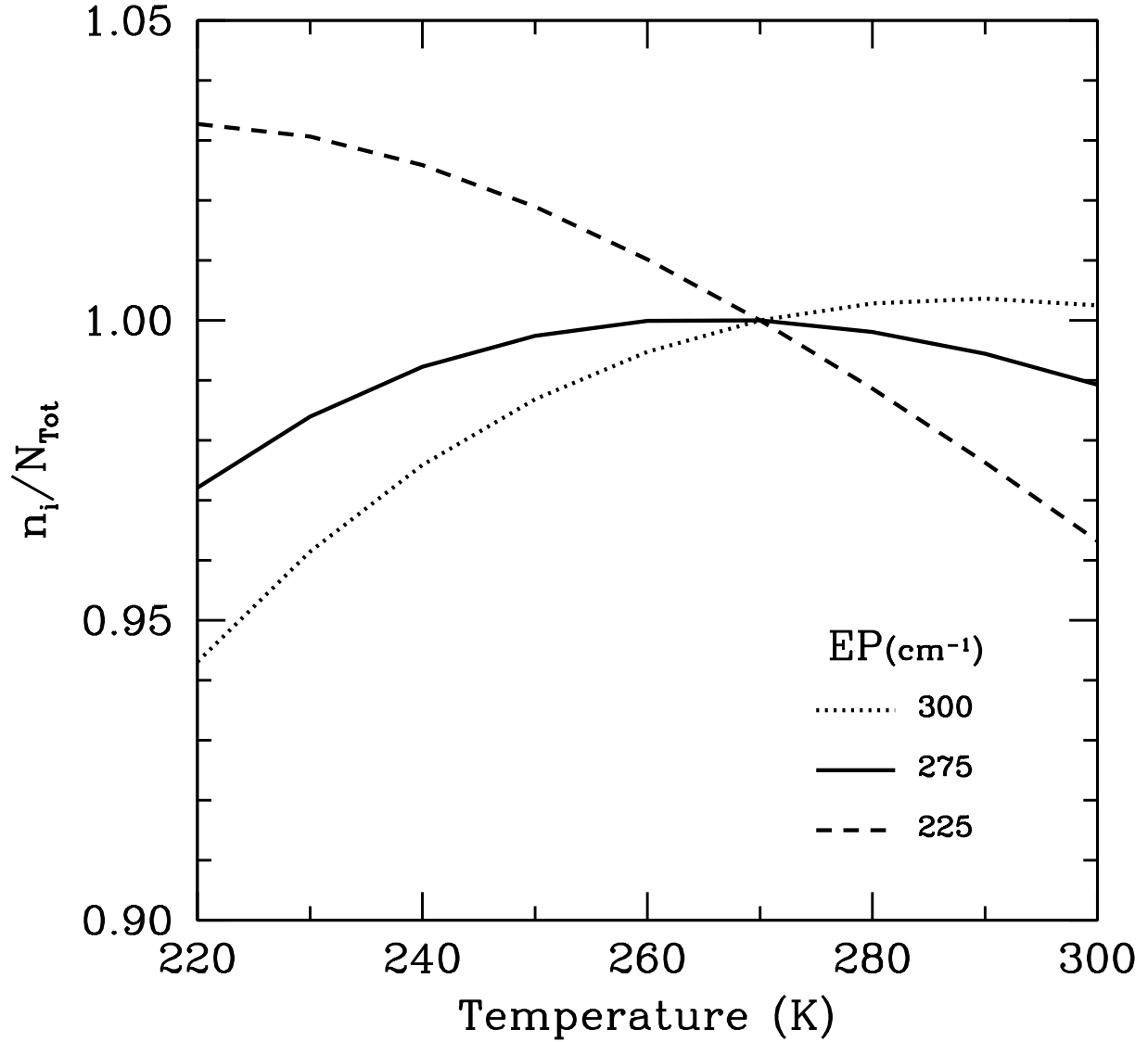


Fig. 3.— A plot showing the fractional population of levels (n_i/N_{tot}) in H_2O as a function of temperature, in the range 220–300 K, for level energies of 225, 275 and 300 cm^{-1} . Over the range of temperatures seen in the earth’s atmosphere the fractional population of levels in this energy level range changes very little, and allows for robust measurement of PWV, without a detailed model atmosphere.

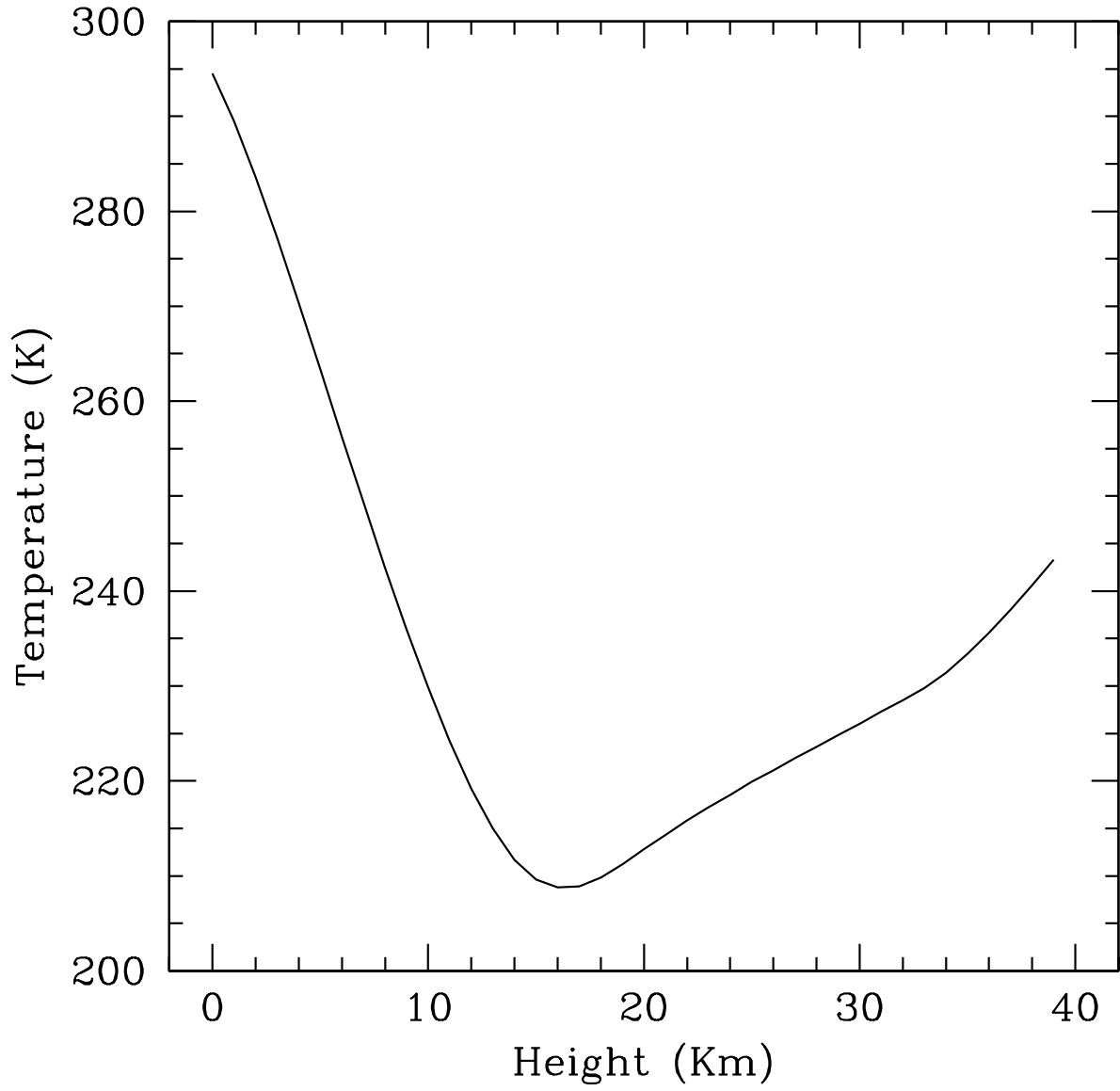


Fig. 4.— MSIS-E-90 model atmosphere

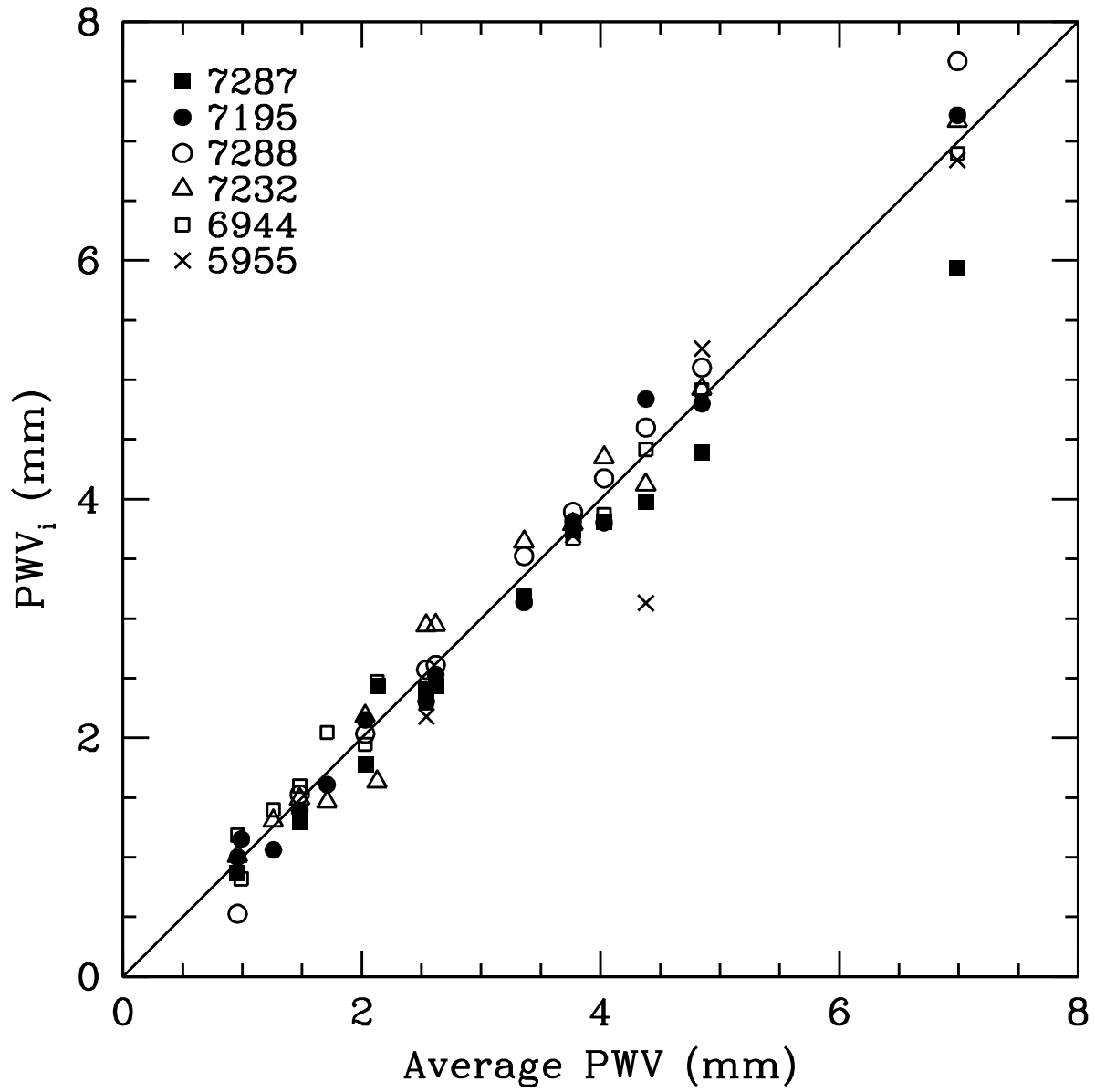


Fig. 5.— A plot showing the individual PWV results from all lines, compared to the average PWV of each spectrum. The straight line corresponds to a 1:1 relation. Symbols for different line wavelengths are indicated top left. There are no unambiguous systematic trends of individual lines deviating from the mean.

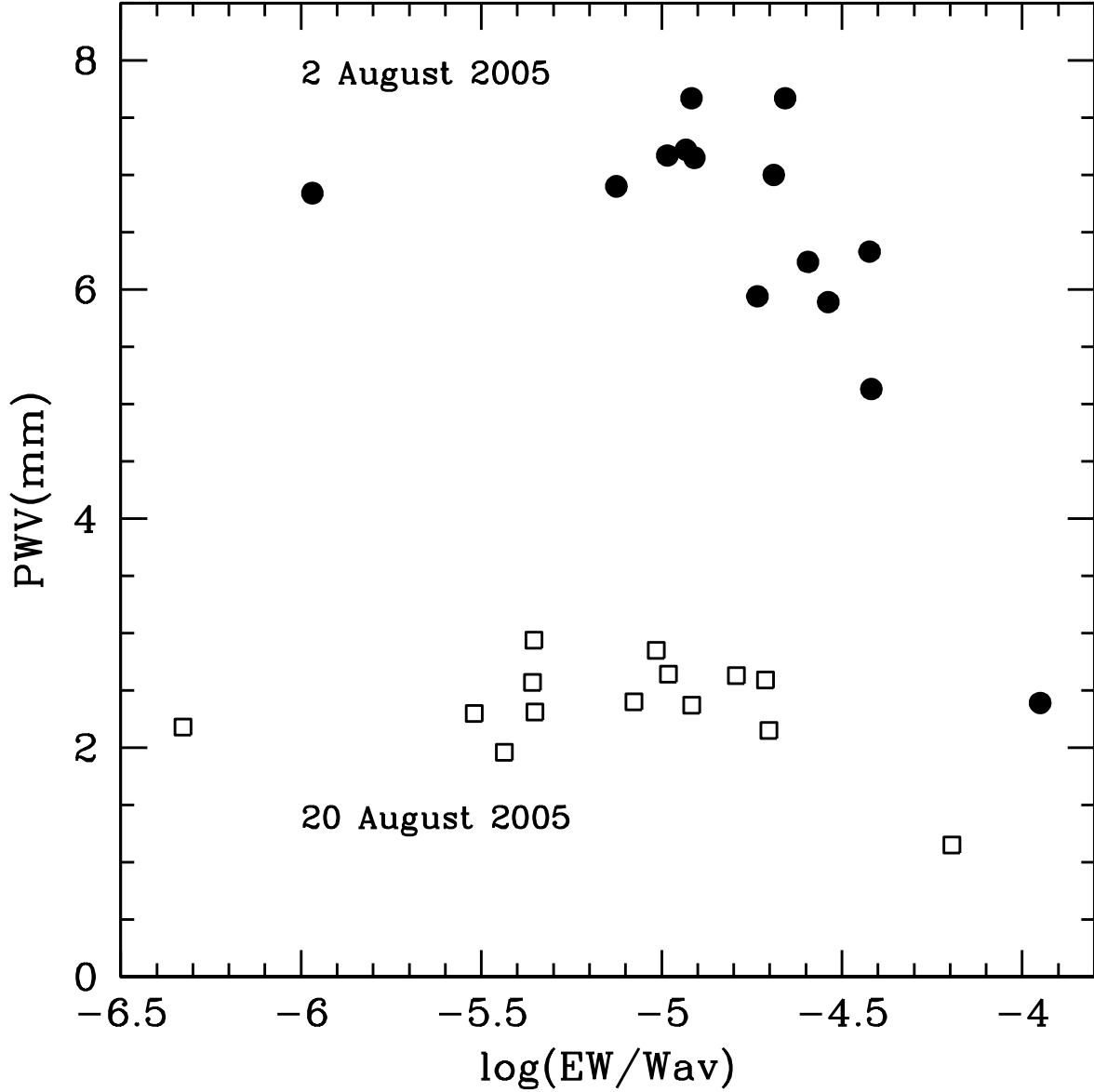


Fig. 6.— A plot showing the results from PWV calculations for strong and weak lines on the wettest night (2 August 2005, filled circles) and a moderately dry night (20 August 2005, open boxes). For the wettest night there is a clear down-turn in the PWV estimates above a reduced equivalent width around -4.6 to -4.7 , indicating that lines above that width suffer from saturation. On the drier night only one line was saturated; the excellent agreement between the unsaturated lines shows that the down-turn of the PWV points for the wettest night was not due to systematic error in line gf values.

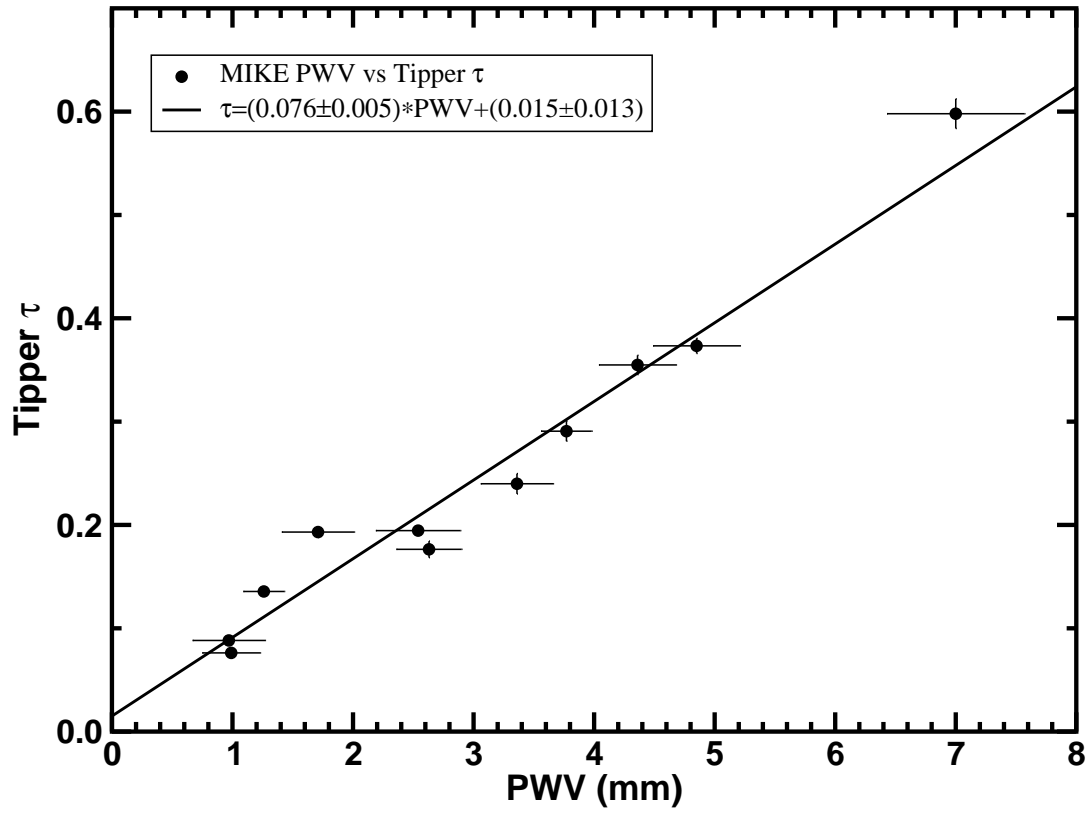


Fig. 7.— The correlation between MIKE echelle PWV Measurements and 225 GHz tipper opacities at LCO during the period between mid-July and mid-Sept 2005. Where no error bars are visible the errors are within the size of the symbol. The line represents a linear least squares fit with characteristics denoted in the legend.

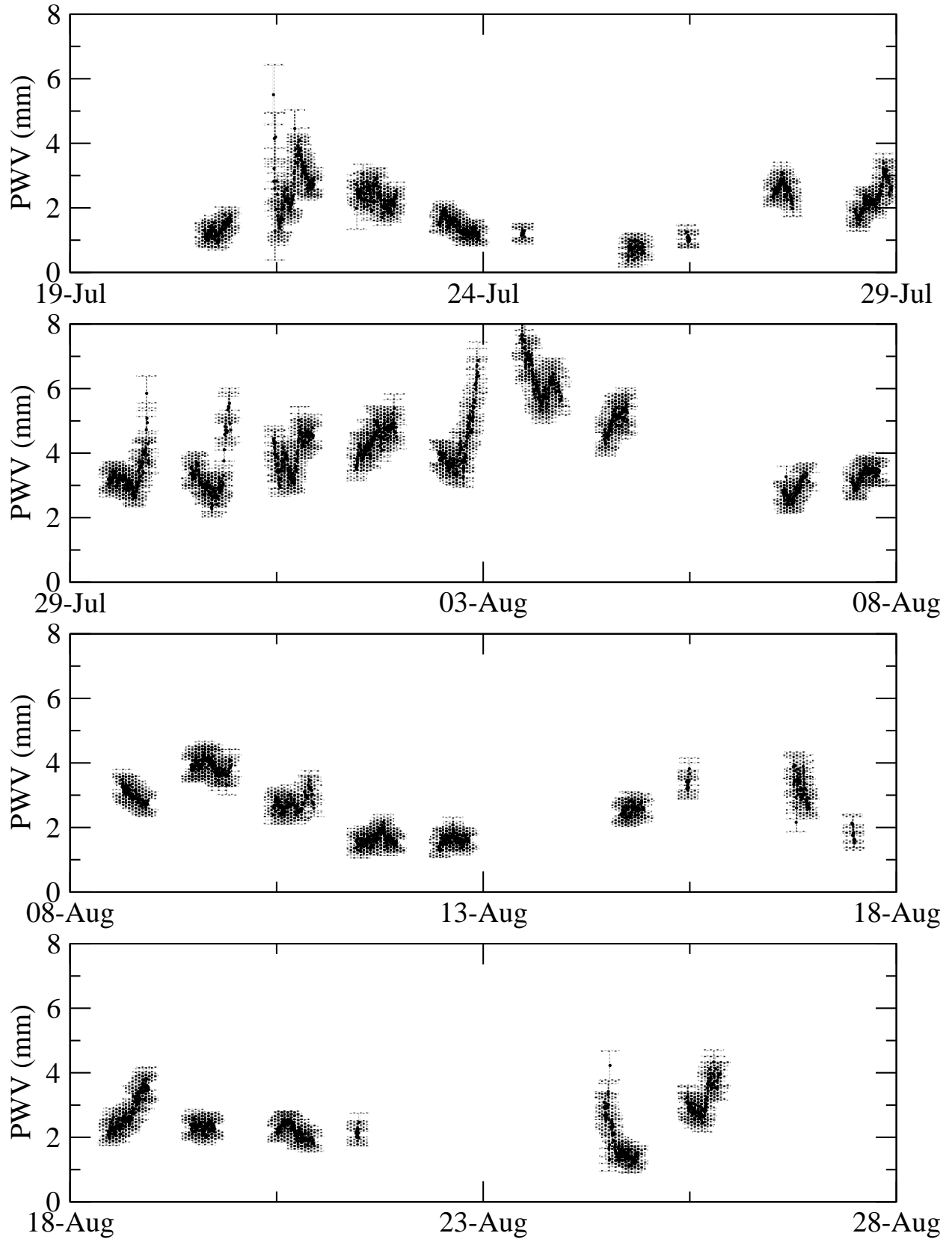


Fig. 8.— Clear night-time PWV as a function of time during our campaign. Uncertainties are indicated in gray.

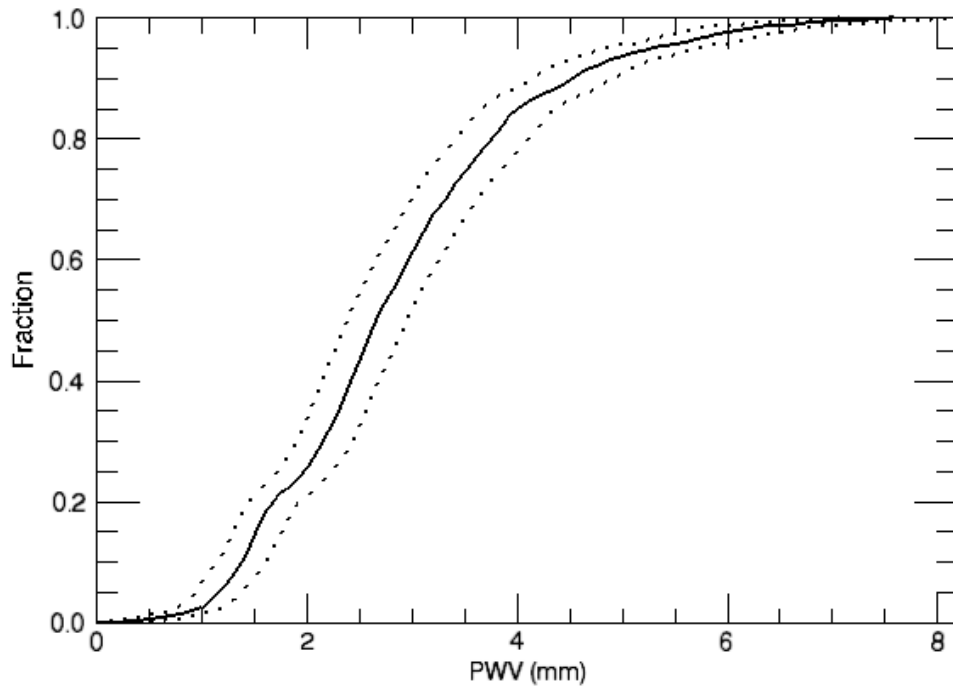


Fig. 9.— Solid line represents the fraction of PWV measurements below a given value. Dotted lines represent the uncertainties due to both the measurements and the calibration. The 10, 25, 50, 75, and 90 percentiles are 1.5, 2.1, 2.8, 3.6, and 4.6 mm, respectively.